PERTURBATION OF A TURBULENT BOUNDARY-LAYER BY A BARCHAN DUNE

Erick de Moraes Franklin, franklin@fem.unicamp.br
Faculdade de Engenharia Mecânica - UNICAMP
Rua Mendeleyev, 200 , Cid. Universitária Zeferino Vaz
Campinas - SP

Abstract. The transport of solid particles entrained by a fluid flow is frequently found in nature and in industrial environments. If shear stresses exerted by the fluid on the bed of particles are bounded to some limits, a mobile layer of particles takes place in which the particles stay in contact with the fixed bed, known as bed-load. If it takes place over a non-erodible ground, and if the particles flow rate is small enough and the fluid flow one-directional, an initial thin continuous layer of particles becomes discontinuous and composed of isolated dunes with a crescentic shape: the barchans. We present here an experimental study concerning the perturbation of a turbulent boundary layer by an isolated barchan dune composed of zirconium beads. In our experiments, the dunes were submitted to a rectangular closed-conduit turbulent water flow. With PIV techniques, we measured the fluid flow perturbation caused by the dune and identified the fluid friction over the dune surface, a key point to understand dune morphology and grains flow rate.

Keywords: Turbulent boundary-layer, bed-load, instabilities, barchan dunes

1. INTRODUCTION

The transport of solid particles entrained by a fluid flow is frequently found in nature and in industrial environments. It is present, for example, in the erosion of bank rivers, in desert dunes displacement, in sand transport in hydrocarbon pipelines and in food industry granular transport. A better knowledge of this kind of transport is then of great importance to understand nature and also to improve particles related industrial procedures. Nevertheless, up to now, it has not been theoretically well understood.

When shear stresses exerted by the fluid flow on the bed of particles are able to move some of them, but are relatively small compared to particles weight, a mobile layer of particles known as bed-load takes place in which the particles stay in contact with the fixed bed. The thickness of this mobile layer is a few particle diameters ([Bagnold (1941)]).

Bed-load existence depends on the balance of two forces: a) an entraining force, of hydrodynamic nature, proportional to τd^2, where τ is the bed shear stress and d is the mean particle diameter; b) a resisting force, in this case related to particles weight, proportional to $(\rho_s - \rho)gd^3$, where ρ is the density of the fluid, ρ_s is the density of the particles and g is the gravitational acceleration.

The relevant dimensionless parameter is the Shields number θ, which is the hydrodynamic force to weight ratio:

$$\theta = \frac{\tau}{(\rho_s - \rho)gd} \tag{1}$$

Bed-load takes place for $\theta = O(0.1)$.

Under the fluid flow, the plane bed may become unstable and deformed, generating dunes. So, if bed-load takes place over a non-erodible ground, as a closed-conduit wall for instance, and if the particles flow rate is small enough, an initial thin continuous layer of particles becomes discontinuous and composed of isolated dunes ([Franklin and Charru (2009)]). In a closed-conduit those isolated dunes generate supplementary pressure loss. Moreover, as they migrate inside the closed-conduit, they may generate pressure fluctuations ([Franklin (2008)]).

The evolution of the fluid flow over the granular bed is of great interest to understand its stability ([Hunt et al. (1988)], [Jackson and Hunt (1975)], [Weng et al. (1991)], [Kroy et al. (2002)]). We present here an experimental study concerning the latter situation. The objective is to understand the influence of isolated dunes in the water flow. This situation, although very common in industrial applications, has not been exhaustively studied. The next section describes the theory concerning the perturbation of a turbulent boundary layer by a hill. It is followed by 2 sections describing the experimental set-up and the experimental results. Follows the conclusions section.

2. PERTURBATION OF A TURBULENT BOUNDARY-LAYER BY A HILL

2.1 Channel flow

The fluid flow close to a wall, in both open and internal flows, has distinct regions. This comes from the fact that its behaviour is not the same very near the surface, where it is slowed down by viscous effects, and far from the surface, were

it is mainly inertial. In between these two regions, there is a matching region. As we are concerned here with channel flows, we will focus our analysis in terms of internal flows. However, the same development can be made for external flows.

Far from the wall, the characteristic velocity is the velocity in the center, U_c, and the characteristic length is the channel height h_{canal}. The mean velocity U in this region can be built as a second order correction of the velocity in the center:

$$\frac{U}{U_c} \sim 1 + \Delta F_1 \tag{2}$$

where Δ is the first term of a gauge function (then, of order 2) and F_1 is a function of Y (of order 1). Y is the coordinate y in terms of external scales:

$$Y = \frac{y}{h_{canal}} \tag{3}$$

In the region very near the wall, the flow is slowed down by viscosity. The scales are then small in this region and the viscous effects cannot be neglected. The velocity scale is a small scale u_* and the length scale is the viscous length, ν/u_*. In this case, the mean velocity U in this region can be considered as proportional to u_*:

$$\frac{U}{u_*} \sim f_0 \tag{4}$$

where f_0 is a function of y^+, the coordinate y in terms of the internal scales:

$$y^+ = \frac{y u_*}{\nu} \tag{5}$$

As we said, it must exist a matching region between those two regions. If we consider the gauge function as $\Delta = \frac{u_*}{U_c}$ and proceed to the matching of the velocities and of their first derivatives, we find the velocity in the matching region. So, in external scales, doing $Y \rightarrow 0$:

$$\frac{U - U_c}{u_*} = \frac{1}{\kappa} \log Y + C_0 \tag{6}$$

and in internal scales, doing $y^+ \rightarrow \infty$:

$$\frac{U}{u_*} = \frac{1}{\kappa} \log y^+ + C_i \tag{7}$$

which gives us the well known *log law*. If we write Eq. 7 with $y_0 = e^{-\kappa C_i}$, we find:

$$U = \frac{u_*}{\kappa} \log(\frac{y}{y_0}) \tag{8}$$

As we will see latter, this is the unperturbed velocity profile in the channel, in the region to be affected by the presence of a dune.

A dimensional analysis with the momentum equation indicates that $u_* = \sqrt{\frac{\tau}{\rho}}$.

2.2 Perturbation of the boundary-layer by a hill

The perturbation of a turbulent boundary-layer by a hill can be found by perturbation methods. This is the case of the series of articles [Jackson and Hunt (1975)], [Hunt et al. (1988)] and [Weng et al. (1991)].

[Jackson and Hunt (1975)] and [Hunt et al. (1988)] analyse the case of a two-dimensional turbulent flow over a plane surface, perturbed by a small aspect ratio hill. If this hill has a height H and a length $2L$ at the half-height (so the total length is $\approx 4L$), a small aspect ratio means $H/L \ll 1$. Considering that the surface rugosity is $z_0 \ll L$, They impose $0 < \ln^{-1}(L/z_0) \ll 1$.

[Jackson and Hunt (1975)] divide the fluid flow in two regions: one external, were the shear stress perturbations, due to the hill, are not important, and the fluid can be treated as inviscid; an internal region, were the shear stress perturbations are important and need to be taken into account. [Hunt et al. (1988)] go further and divide each of these regions into two layers.

[Jackson and Hunt (1975)] and [Hunt et al. (1988)] find that, in the external region, the velocity and pressure perturbations in the first order are irrotational and not related to the boundary-layer thickness, so that they correspond to the classical solution to the potential problem. On the other hand, in the next order, these perturbations are affected by the upstream velocity gradient and by the boundary-layer thickness. The solution of the external region is then the solution

of the potential case corrected, in the next order, by the inertial effects of turbulence. This correction has minor effects in the magnitude of the inviscid perturbations, but it causes an upstream shift, making them out of phase with respect to the hill. The perturbations of speed and shear stress over the surface are (in Fourier space):

$$\hat{u}(k, Z) = \frac{H/L}{U(h_i)}\sigma(k)(1 + \epsilon(1 - 2\ln(Z/h_i) - 4K_0)) \tag{9}$$

$$\hat{\tau}(k, Z = 0) = \frac{2H/L}{U^2(h_i)}\sigma(k)(1 + \epsilon(2\ln k + 4\gamma_E + 1 + i\pi)) \tag{10}$$

where $\epsilon = \ln^{-1}(h_i/z_0)$; $Z = z - Hf(x/L)$ is a displaced scale; γ_E is the Euler constant; K_0 is a modified Bessel function, with argument $2\sqrt{ikZ/h_i}$ and $\sigma(k)$ is the Fourier transform of $\sigma(x/L)$, the normalised pressure perturbation:

$$\sigma(x/L) = \frac{1}{\pi} \int_{-\infty}^{\infty} \frac{f'(x^+/L)}{(x - x^+)} dx^+ \tag{11}$$

The solution of [Jackson and Hunt (1975)] and [Hunt et al. (1988)] are carried on by [Weng et al. (1991)] to obtain the shear stress perturbations over a barchan dune. They divide the fluid flow over the dune in the same regions as in [Hunt et al. (1988)], but the computations consider a three-dimensional flow. They find the following expression for the surface shear stress in the longitudinal and transverse directions, respectively:

$$\hat{\tau}_x(k, z = 0) = \frac{\tilde{f}k_x^2}{|k|}\frac{2}{U^2(h_i)}\left(1 + \frac{2\ln(|k_x|) + 4\gamma_E + 1 + i\pi}{\ln(h_i/z_0)}\right) \tag{12}$$

$$\hat{\tau}_y(k, z = 0) = \frac{\tilde{f}k_x k_y}{|k|}\frac{2}{U^2(h_i)} \tag{13}$$

where $\tilde{f}$ is the two-dimensional Fourier transform of the hill and k_x and k_y are the wave-numbers in the longitudinal and transverse directions, respectively. Again, the solution of the external region is the solution of the potential case corrected, in the next order, by the inertial effects of turbulence. This correction has minor effects in the magnitude, but it causes an upstream shift.

[Sauermann (2001)] and [Kroy et al. (2002)] propose simplified versions of equations 12 and 13. By a dimensional analysis, they show that the longitudinal shear stress can be expressed in Fourier space as :

$$\hat{\tau_k} = Ah(|k| + iBk) \tag{14}$$

and in real space:

$$\hat{\tau}_x = A\left(\frac{1}{\pi}\int\frac{\partial_x h}{x - \xi}d\xi + B\partial_x h\right) \tag{15}$$

where A and B are considered as constants, as they vary as the logarithm of L/z_0

Equations 14 and 15 show, in a simple way, the form of the flow perturbation by a hill (or dune). The first term in the RHS of equation 15, the convolution product, is symmetric, similar to the potential solution of the perturbation over a hill. It comes from the pressure perturbations caused by the hill. The second term in the RHS of equation 15, which takes into account the local slope, is anti-symmetric. It comes from the non-linear inertial terms of the turbulent flow and can be seen as a second order correction of the potential solution, with minor changes in the magnitude of the first order solution, but causing an upstream shift.

Also, [Sauermann (2001)] and [Kroy et al. (2002)] argue that the recirculation region must be taken into account in Eqs. 14 and 15. They propose that h must be built as the surface of the hill plus the boundary of the recirculation region.

3. EXPERIMENTAL SET-UP

A closed-conduit experimental loop of rectangular cross-section (for simplicity, we name it "channel" in the following) and made of transparent material was used to investigate the perturbation of a water flow by a barchan dune.

Concerning the fluid flow, we are interested here in the fully turbulent regime. This can be defined in terms of the Reynolds number based on the cross section average velocity $\bar{U}$ and on the conduit height H: $Re = \frac{\bar{U}H}{\nu} > 10000$, where ν is the kinematic viscosity. In the turbulent case, the shear velocity u_* is defined by $\tau = \rho u_*^2$.

In our experiments we employed water as the fluid media and some beads as granular media: glass beads with density $\rho_s = 2500 kg/m^3$ and mean diameter $d = 0.5\, mm$, $d = 0.2\, mm$ and $d = 0.12\, mm$ and zirconium beads with density
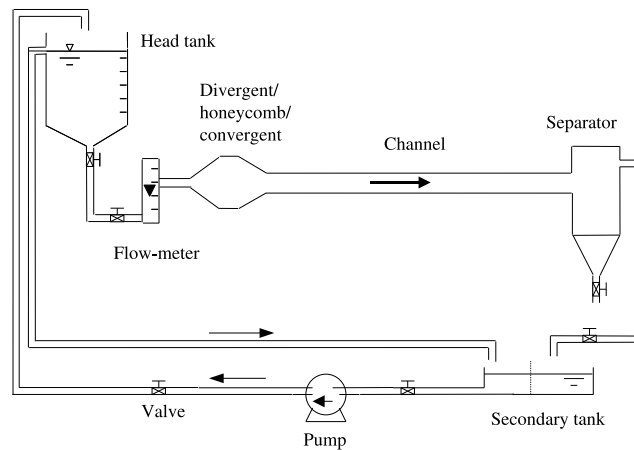
Figure 1. Experimental equipment.

$\rho_s = 3800 kg/m^3$ and mean diameter $d = 0.19\,mm$. Water flow rate varied between $6\,m^3/h$ and $10\,m^3/h$, what gives us the following range of Shields number θ and Reynolds number Re: $0.02 < \theta < 0.41$ and $13000 < Re < 24000$.

In order to have a good control of dunes displacement and deformation under a permanent water flow, it is desirable to have low turbulence levels at the channel inlet. This was achieved by establishing a gravitational flow by means of a constant level head tank rather than the direct use of a pump.

The experimental loop is made of (figure 1):

1) A head tank. This constant water level tank gives a $2\,m$ head pressure at the channel (test section). Water is continuously pumped to the tank (from the secondary tank) and the level is assured constant by an overflow passage (discharging in the secondary tank).

2) An electromagnetic flow-meter, which measures the fluid flow rate in the channel.

3) A divergent/honeycomb/convergent device, which can break large turbulent structures.

4) An horizontal channel (test section).

5) A fluid-particles separator. Particles settle due to a strong expansion (velocity reduction) of the fluid flow.

6) A secondary tank. The channel fluid flow and the head tank overflow are discharged in this tank. Water is continuously pumped from this tank to the head tank.

7) A water lifting pump, which continuously pumps water from the secondary tank to the head tank. The pumped water flow rate is larger than the water flow rate in the channel, maintaining the head tank water at a constant level.

8) Some valves to control the water flow rate.

The channel is a six meters long horizontal closed-conduit of rectangular cross-section ($120\,mm$ wide by $60\,mm$ high), made of transparent material. One of the advantages of the rectangular cross-section channel is its plane horizontal surface. The fluid flow in this kind of channel is well-known ([Melling and Whitelaw (1976)]).

The experimental procedure was as follows: a conical pile of beads was built, from a funnel, in the channel (already filled up with water). The funnel was located at $4.15\,m$ from the channel inlet. Then, a constant fluid flow was established. The conical pile rapidly became a barchan dune and the motion of it was recorded by a camera and the fluid flow measured by a PIV device. With this procedure, each experiment concerns one single isolated dune.

A mirror inclined at 45° made it possible the use of one single camera to obtain top and profile images of barchan dunes. The camera, mounted on a rail system, was above the channel and had a direct top view of the dune. The mirror, close to one of the vertical sides, indirectly provided the dune profile image to the camera. As the camera was mobile and as a rule was fixed on the channel, one could follow each barchan dune and record its displacement and deformation. A description of this device can be seen in [Franklin and Charru (2007)] and [Franklin and Charru (2009)]. An example of image obtained by it can be seen in the left part of figure 2: top view on the right and side view on the left.

Another camera and the PIV laser head were attached to a $3-D$ translation device, so that we could follow the barchan dune as it migrate downstream. Also, with this device, we were able to make a laser sheet in the vertical symmetry plane of the channel or in the symmetry plane of the barchan dune, which were our regions of interest.

The PIV (Particle Image Velocimetry) measurements were performed to find the fluid velocity profile $u(y)$ and the shear velocity u_* on the vertical symmetry plane of the channel, for a mono-phase water flow, but also to find the fluid velocity profile $u(y)$ and the shear stresses over the dune surface. A layout of the PIV apparatus can be seen in the right part of figure 2.

In the case of mono-phase water flow (unperturbed flow) we used a 1280×1024 pixels CCD camera to record a total field of $85\,mm \times 68\,mm$. As the vertical direction of the total field was larger then the channel height H, the effective

Figure 2. In the left, example of image obtained by the camera/mirror device (on the right we have a direct top view of the barchan dune by the camera and on the left we can see the barchan profile reflected by the mirror and indirectly caught by the camera). The fluid flow is from top to bottom. In the right, PIV experiment layout.

field corresponds to $85\,mm \times 60\,mm$. To the PIV calculations we used a 16×16 pixels interrogation area, without overlaping, which, considering the total field, corresponds to a resolution of $1.06\,mm \times 1.06\,mm$.

In the case of water flow over a dune (perturbed flow) we used a 1280×1024 pixels CCD camera to record a total field of $37\,mm \times 27\,mm$ and $22\,mm \times 17\,mm$. To the PIV calculations we used a 16×16 pixels interrogation area with an overlap of 50%, which, considering the total field, corresponds to resolutions of $0.21\,mm \times 0.21\,mm$ and $0.14\,mm \times 0.14\,mm$, respectively.

4. RESULTS

4.1 Unperturbed flow

We are interested here in turbulent fluid flows in rectangular channels. Many previous works were done on this subject. For instance, [Melling and Whitelaw (1976)] studied a turbulent water flow in a closed-conduit of rectangular cross-section, what is similar to our case. In the vertical symmetry plane, they found a turbulent boundary layer, with the typical logarithmic layer, close to the channel walls. On the other vertical planes parallel to the symmetric one, they found the same kind of profile, with only slight changes, except very near the vertical walls of the channel (within 5% of the channel width). As in our experiments dunes occupied the central part of the channel, we considered the fluid flow in the vertical symmetry plane as being characteristic of the unperturbed flow in the channel.

To this experiments, we were interested in finding the mean quantities but also the fluctuations of a permanent turbulent water flow. This means that we needed a certain amount of measurements to assure average and fluctuations convergence. Also, because dunes formation and displacement have long time scales compared to the fluid flow time scales, we sampled the flow with a time interval allowing non-correlated measurements in time. The information concerning the fluid flow conditions and PIV sampling can be seen in Tab. 1

Q_L m^3/h	U_{deb} m/s	U_{moy} m/s	Re $\cdots$	Re_{dh} $\cdots$	f Hz	Δt μs	N $\cdots$
$6,0$	$0,23$	$0,24$	13900	18500	4	848	215
$6,5$	$0,25$	$0,26$	15000	20100	4	848	215
$7,0$	$0,27$	$0,29$	16200	21600	4	848	1074
$7,5$	$0,29$	$0,31$	17400	23100	4	848	215
$8,0$	$0,31$	$0,33$	18500	24700	1	848	1074
$8,5$	$0,33$	$0,35$	19700	26200	4	848	1074

Table 1. Unperturbed flow PIV. Q_L is the water flow rate (from the flow-meter), U_{deb} is the mean velocity computed from the flow-meter and the transversal section, U_{moy} is the mean velocity computed from the PIV measurements in the channel vertical symmetry plane, Re is the Reynolds number based on the channel height, Re_{dh} is the Reynolds number based on the hydraulic diameter, f is the frequency sampling of the image pairs, Δt is the time interval between images of the same pair and N is the total number of image pairs (displacement fields).

All those mean velocity profiles (in the symmetry plane) can be seen in Fig. 3a. The profiles are seen to be symmetric about the channel axis and fully developed. Given the interrogation area, the distance between each measured point is

approximately $1\,mm$. The legend in the figure corresponds to Re.

Figure 3b shows the low half of those vertical profiles in a semi-logarithmic scale (y^+ is in logarithmic scale). We can see that this half-profile follows a logarithmic law, with a matching region in the channel axis (y around $30\,mm$) and an "internal" region (in fact, the buffer layer) close to the horizontal faces. So, in the vertical symmetry plane, we have two logarithmic profiles beginning on the horizontal faces and matching each other at the channel axis. The u_* values can easily be found from this kind of profile. They correspond to the mono-phase water flow shear on the horizontal walls of the channel, in the vertical symmetry plane. Note that it is different from the u_* over the dune itself. In fig. 3b, the vertical distance from the bottom wall was non-dimensionalysed by the viscous length $y^+ = yu_*/\nu$ and the longitudinal velocity was non-dimensionalysed by the friction velocity $u^+ = u/u_*$

Figure 3. (a) mean longitudinal velocity profile in linear scale. (b) mean longitudinal velocity half-profile in semi-logarithmic scale. Symbols in the figure correspond to Re. $y^+ = yu_*/\nu$ and $u^+ = u/u_*$.

Figure 4 shows Reynolds stresses $-\rho\overline{u'v'}$ divided by ρu_*^2. These profiles are in good agreement with the literature. We can observe the anti-symmetry of the profiles, with positive values in the bottom and negative on the top. In the central part, the variation of the profiles is linear and the value of $-\rho\overline{u'v'}$ in the center is zero. If we associate, far from the walls, $-\rho\overline{u'v'}$ to the total stress, these profiles agree very well with the mean velocity profiles: a linear behaviour in the central part of the channel and a zero value in the center (where the mean velocity gradients are zero).
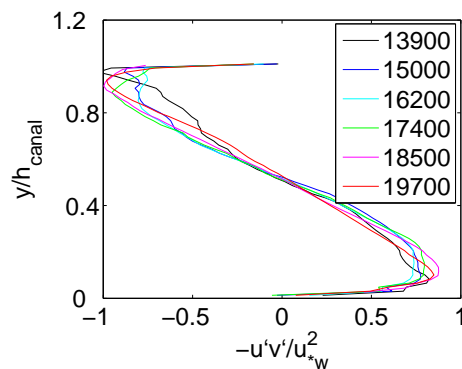
Figure 4. $-\rho\overline{u'v'}$ profiles non-dimensionalysed by ρu_*^2. The Reynolds numbers Re are shown in the legend.

Close to the walls we can see that, after reaching a maximum, the $-\rho\overline{u'v'}$ profiles go to zero as we get close to the walls: it is in this region that the viscous stresses are of the same order of magnitude as the turbulent stresses. In this region, the fluctuations of u' and v' become out of phase, decreasing the values of $-\overline{u'v'}$ and the fluctuations need to become zero on the walls, so $u' \to 0$ and $v' \to 0$ when $y/h_{canal} \to 0$ or $y/h_{canal} \to 1$.

To summarise the non-perturbed flow, we saw that the mean velocity profiles are symmetric and in good agreement with turbulent boundary layer profiles, with a viscous region, a buffer region, a logarithmic region and an external region (core flow). The velocity fluctuations are also symmetric and, again, in good agreement with a turbulent boundary-layer.

4.2 Perturbed flow

In order to increase the spatial resolution, the total field of the PIV measurements of the perturbed flow was decreased. It was of $34\,mm \times 27\,mm$ or of $22\,mm \times 17\,mm$. As the dunes in the channel had a length of some tens of mm, the total field wasn't able to measure the flow over an entire dune. To solve this problem, the laser head and the camera were fixed to three-dimensional translation devices, so that we could displace the field over the entire dune.

In some cases, we were only interested in the perturbed flow by the form of the dune, without bed-load occuring
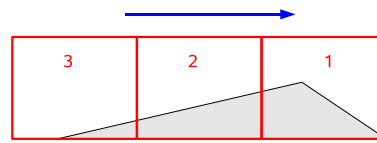
Figure 5. Identification of different fields over the dune.

on its surface. In those cases, the fluid flow was, once the dune formed, brought down to a value under the threshold (experiments with fixed grains, $Re = 9300$).

To the PIV calculations we used a 16×16 pixels interrogation area with an overlap of 50%, which, considering the total fields of $34\,mm \times 27\,mm$ and $22\,mm \times 17\,mm$, corresponds to resolutions of $0.21\,mm \times 0.21\,mm$ and $0.14\,mm \times 0.14\,mm$, respectively.

In order to limit the displacement of the dunes during the PIV images acquisition, we employed only zirconium beads to form the dunes, which correspond to the slowest dunes. However, the acquisition frequency was limited to $4\,Hz$. This limits the total number of images to be employed in the computations in cases where the fluid flow was too strong. Table 2 presents the acquisition parameters.

Q_L m^3/h	Re $\cdots$	f Hz	Δt μs	$N1$ $\cdots$	$N2$ $\cdots$	$N3$ $\cdots$
4	$0,9 \cdot 10^4$	4	496	864	864	432
6	$1,4 \cdot 10^4$	4	288	432	432	432
7	$1,6 \cdot 10^4$	4	256	216	216	216
8	$1,9 \cdot 10^4$	4	224	108	108	$\cdots$

Table 2. PIV parameters for the perturbed flow. Q_L is the water flow rate, Re is the Reynolds number based on the channel height, f is the acquisition frequency of image pairs, Δt is the time interval between images of the same pair and $N1$, $N2$ and $N3$ are the number of images employed in the computations concerning each part of the dune (from the top of the dune to its toe, parts 1, 2 and 3, respectively: Fig. 5).

An easy way to see how the fluid flow perturbation looks like is by tracing the streamlines of the mean flow. This is shown in fig. 6 for two cases: one where there is no bed-load, $Re = 9300$ and another where there is bed-load over the dune surface, $Re = 13900$.

Figure 6. Lower half of the mean velocity field above a barchan dune, in terms of streamlines. In the left, $Re = 9300$ and there is no bed-load. In the right, $Re = 13900$ and there is bed-load. Streamlines are shown here with the half of PIV resolution.

These streamlines show us some basic characteristics of the perturbation. They show us the form of the fluid flow perturbation, indicated by the curvature of the streamlines. The fluid flow is much more perturbed downstream the dune crest, where we can see a strong recirculation region: it is the reason why the grains in the front of the dune stay trapped and are not entrained downstream, avoiding the dune vanish. One can also see that the perturbation is similar in the two cases, indicating that the perturbation due to the dune shape is greater than the one related to the existence of bed-load. For this reason, only the measurements concerned with dunes with bed-load (case in which we are interested in) will be shown in this paper.

Figure 7. Some profiles of the mean longitudinal velocity over a barchan dune, in semi-logarithmic scale : $Re = 13900$. The legend indicates the longitudinal positions where the profiles were taken, 0 being the position of the crest.
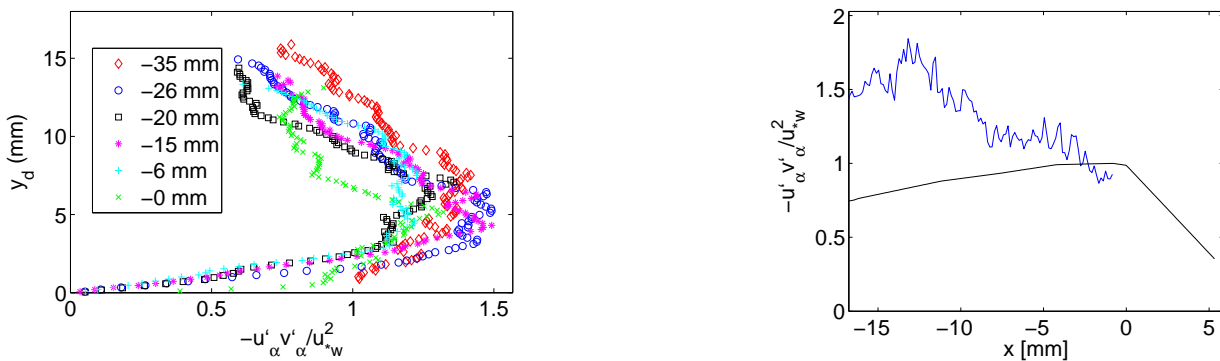
Figure 8. In the left, some Reynolds stresses profiles non-dimensionalysed by the square of the friction velocity of the unperturbed flow, $-\overline{u'_\alpha v'_\alpha}/u^2_{*w}$, in the case where $Re = 13900$ and $u_{*w} = 0,0130\,m/s$. In the right, longitudinal evolution of the $-\overline{u'_\alpha v'_\alpha}/u^2_{*w}$ maxima, when $Re = 18500$ and $u_{*w} = 0,0168\,m/s$.

Figure 7 show us some profiles of the mean longitudinal velocity over a barchan dune in semi-logarithmic scale, in terms of y and y_d. y is the absolute vertical coordinate (its origin is in the bottom of the channel) and y_d is a displaced coordinate, with origin at the surface of the dune: $y_d = y - h(x)$, where $h(x)$ is the local height of the dune.

With this isolated profiles, we can get more information about the perturbation of the fluid flow than in the case of streamlines. From the y profiles, we can observe 3 distinct layers: an inner layer close to the dune surface, where there are strong velocity gradients; an intermediary layer between the inner one and the top of the profiles, were there is an advective acceleration; an external layer, weakly perturbed at its top, where the profiles are logarithmic and close to the ones measured without dunes in the channel (unperturbed flow). From the y_d profiles, we can quantify the thickness of these layers: we have an inner layer within $y_d < 1\,mm$, the intermediary layer within $1\,mm < y_d < 10\,mm$ and the external layer within $y_d > 10\,mm$.

With the number of image pairs we acquired from the PIV measurements (Tab. 2), we were able compute the second order momentum quantities. One of the main quantities we are concerned here is the Reynolds stress component in the plane of measurement, $-\rho\overline{u'v'}$. Because we are dealing with a turbulent boundary layer, we can associate the maximum value of this quantity to the shear stress at the dune surface, which is the key parameter to understand the bed-load transport over the dune and the related instabilities.

The left part of Fig. 8 shows some Reynolds stresses profiles non-dimensionalysed by the square of the friction velocity of the unperturbed flow, $-\overline{u'_\alpha v'_\alpha}/u^2_{*w}$. The subscript α means that the coordinate system is related to the dune surface (in fact, α is the local slope of the dune surface). From these profiles, we can see that $-\overline{u'_\alpha v'_\alpha}/u^2_{*w}$ reaches a maximum value at a certain distance from the dune surface, going very fast to zero as we approach the dune surface (due to u' and v' becoming out of phase and also tending to zero), and tending to zero linearly as we approach the center of the channel. If we consider that we have a full turbulent boundary layer near the dune surface, we can associate the maxima of the Reynolds stresses to the total stress acting on the surface of the dune: The Reynolds stress maxima occur very near the dune surface: at this height the viscous contribution to shear stress is negligible. Viscous contribution become important below this height and, as the total shear stress in this region shall be constant, we decided to keep the Reynolds stress maxima as representative of the shear stress on the surface.

The evolution of the fluid stresses is of great importance to the granular bed stability, which may be understood based on the grains flow rate. The mass conservation of the grains in the granular bed link the height of the bed to the grains flow rate: it shows that there is erosion where the gradient of the grains flow rate is positive and deposition where the gradient
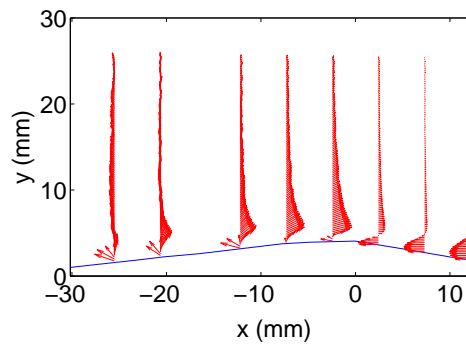
Figure 9. Profiles of the velocity "surplus" over a barchan dune.

of the grains flow rate is negative. So, the stability may be viewed as a question of phase lag: if the maximum of the grains flow rate is upstream a crest, there is deposition at the crest and the bed is unstable. On the contrary, if the maximum of the grains flow rate is downstream a crest, there is erosion at the crest and the bed is stable. To answer the question of the instability conditions, we shall seek the mechanisms creating a phase lag between the shape of the granular bed and the grains flow rate. They are three: the fluid flow perturbation, the relaxation effects and the gravity.

To understand the instabilities giving rise to dunes and ripples, it is very important to know the longitudinal evolution of the Reynolds stresses ([Franklin (2008)] and [Franklin and Charru (2007)]). If we consider that the grains flow rate is proportional to the fluid shear stresses, and that the fluid shear over a hill is out-of-phase (upstream shift), then the perturbation of the fluid flow is the unstable mechanism. On the other hand, relaxation effetcs and the gravity are the stable mechanisms.

We present in the right part of Fig. 8 the the longitudinal evolution of the $-\overline{u'_\alpha v'_\alpha}/u^2_{*w}$ maxima. Based on the considerations concerning the shear stress on the dune surface (just described), we see from this figure that the maximum of the fluid flow shear stress is shifted upstream, which agrees with the theoretical analysis ([Hunt et al. (1988)], [Jackson and Hunt (1975)], [Kroy et al. (2002)], [Weng et al. (1991)]). The experimental finding of this shift of the shear stress is very important to understand why solid grains settle on the crest of the dune, so that its form persists in time. Analysing the totality of our data (not shown here), the shear stress maxima reach a value equal to $1, 3$ times the shear stress of the unperturbed flow (on the channel wall), and is displaced upstream with a length scaling with the barchans minimum size ([Franklin (2008)], [Franklin and Charru (2009)]).

A way to visualise the different regions of the flow perturbed by a hill is by computing the "surplus" of the mean velocities, as done by [Hunt et al. (1988)] and [Jackson and Hunt (1975)]. As we are concerned here with the region close the dune surface, we define the surplus $\Delta \vec{U}$ as the difference between the mean velocities measured over the dune $\overline{U}_{dune}$ and the mean velocities measured without the presence of dunes (unperturbed flow) $\overline{U}_{channel}$, in the displaced coordinate system $y_d = y - h(x)$:

$$\Delta \overline{U}(x, y_d) = \overline{U}_{dune}(x, y_d) - \overline{U}_{channel}(y_d) \tag{16}$$

where $\overline{U} = U\vec{e}_x + V\vec{e}_y$.

Figure 9 shows some velocity "surplus" profiles $\Delta \overline{U}$ in the symmetry plane of a barchan dune. We can distinguish 2 different layers of the perturbation:

- an "inviscid" layer, far from the dune crest $y_d > 10\,mm$, where the fluid flow perturbation is weak. In this region, the perturbation of $u'v'$ is negligible, the longitudinal velocity profiles are logarithmic and the perturbations vanish with y_d increasing;

- a "viscous" layer ($y_d < 10\,mm$), strongly perturbed by the presence of a dune, where $u'v'$ perturbations are very important. In this region, due to the dune shape, there is a strong advective acceleration of the mean flow. The maximum of this acceleration occurs upstream the dune crest. On the bottom of this layer, very near the surface ($y < 0, 5mm$), there is a negative velocity "surplus": this is the effect of the rugosity change from the channel wall (acrylic) to the dune surface (zirconium beads).

5. CONCLUSION

The transport of solid particles as bed-load may, in some cases, give rise to isolated dunes, which are displaced and deformed by the fluid flow. In a closed-conduit, such as hydrocarbon pipelines, those isolated dunes generate supplementary pressure loss. Moreover, as they migrate inside the conduit, they may generate pressure fluctuations. A better understanding of dunes migration is a key point to control sediment transport, as well as to understand nature.

We have investigated experimentally the fluid flow perturbation caused by a barchan dune in a channel flow. To form the dune, an initial pile of beads was placed in the channel, which was rapidly deformed by the water flow, adopting a "croissant" shape, like barchan dunes found in deserts at a much larger scale. As the transport mechanism is quite different in air and in water, those similarities between aeolian and aquatic barchans indicate that their shape is independent of the transport mechanism.

Acquired data shown in this paper concerns PIV measurements of the fluid flow perturbation caused by the presence of a barchan dune in a closed-conduit water flow. The perturbed fluid flow was then compared to the water flow measured in the same channel, without the presence of dunes. The flow was varied in the range $13000 < Re < 24000$.

The measurements show that the fluid flow perturbation is out-of-phase with the dune shape: longitudinal velocities and shear stresses maxima are shifted upstream, agreeing with theoretical analysis. This is very important to understand dune stability. We can summarise the main characteristics of the fluid flow over a barchan dune as follows:

- There is a strong recirculation region downstream the dune crest, with a length scale of the order of the dune length.

- The mean velocity profiles are not logarithmic near the dune surface.

- The shear stresses maxima are displaced upstream the dune crest.

- There are at least 2 distinct layers (fig. 9):

    - an "inviscid" layer, far from the dune crest $y_d > 10\,mm$, where the fluid flow perturbation is weak. In this region, the perturbation of $u'v'$ is negligible, the longitudinal velocity profiles are logarithmic and the perturbations vanish with y_d increasing;
    - a "viscous" layer ($y_d < 10\,mm$), strongly perturbed by the presence of a dune, where $u'v'$ perturbations are very important. In this region, due to the dune shape, there is a strong advective acceleration of the mean flow. The maximum of this acceleration occurs upstream the dune crest. The shear stress maxima reach a value $1,3$ times the shear stress of the unperturbed flow (on the channel wall), and is displaced upstream with a length scaling with the barchans minimum size ([Franklin (2008)], [Franklin and Charru (2009)]).

Measurements of the field of perturbed fluid flow over a barchan dune, in situations where bed-load is present, were performed for the first time in this work. These experimental results are very important to understand dune instability: it is the upstream shift of the shear stress maximum that explains why grains settle on the dune crest.

6. ACKNOWLEDGEMENTS

7. REFERENCES

Bagnold, R.A., 1941, "The physics of blown sand and desert dunes", Ed. Chapman and Hall, London, England.

Franklin, E.M., 2008, "Dynamique de dunes isolées dans un écoulement cisaillé", PhD. Thesis, Université de Toulouse III.

Franklin, E.M.. and Charru, F., 2007, "Dune Migration in a Closed-conduit Flow", Proceedings of the International Conference in Multiphase Flow, Leipzig, Germany.

Franklin, E.M.. and Charru, F., 2009, "Morphology and displacement of dunes in a closed-conduit flow", Powder Technology, Vol.190, pp. 247-251.

Hunt, J.C.R., Leibovich, S. and Richards, K.J., 1988, "Turbulent shear flows over low hills", Quarterly Journal of the Royal Meteorological Society, Vol.114, pp. 1435-1470.

Jackson, P.S. and Hunt, J.C.R., 1975, "Turbulent wind flow over a low hill", Quarterly Journal of the Royal Meteorological Society, Vol.101, pp. 929-955.

Kroy, K., Sauermann, G. and Herrmann, H.J., 2002, "Minimal model for aeolian sand dunes", Physical Review E, Vol.66, 031302.

Melling, A. and Whitelaw, J.H., 1976, "Turbulent flow in a rectangular duct", Jounal of Fluid Mechanics, Vol.778, pp. 289-315.

Sauermann, G., 2001, "Modeling of wind blown sand and desert dunes", PhD Thesis.

Weng, W.S., Hunt, J.C.R., Carruthers, D.J., Warren, A., Wiggs, G.F.S., Livingstone, I. and Castro, I, 1991, "Air flow and sand transport over sand-dunes", Acta Mechanica, Suppl 2, 1, pp. 1-22.

8. Responsibility notice

The author(s) is (are) the only responsible for the printed material included in this paper